

Review

Modeling Calcium Cycling in the Heart: Progress, Pitfalls, and Challenges

Zhilin Qu ^{1,2,*} , Dasen Yan ³ and Zhen Song ³

¹ Department of Medicine, David Geffen School of Medicine, University of California, A2-237 CHS, 650 Charles E. Young Drive South, Los Angeles, CA 90095, USA

² Department of Computational Medicine, David Geffen School of Medicine, University of California, Los Angeles, CA 90095, USA

³ Peng Cheng Laboratory, Shenzhen 518066, China

* Correspondence: zqu@mednet.ucla.edu

Abstract: Intracellular calcium (Ca) cycling in the heart plays key roles in excitation–contraction coupling and arrhythmogenesis. In cardiac myocytes, the Ca release channels, i.e., the ryanodine receptors (RyRs), are clustered in the sarcoplasmic reticulum membrane, forming Ca release units (CRUs). The RyRs in a CRU act collectively to give rise to discrete Ca release events, called Ca sparks. A cell contains hundreds to thousands of CRUs, diffusively coupled via Ca to form a CRU network. A rich spectrum of spatiotemporal Ca dynamics is observed in cardiac myocytes, including Ca sparks, spark clusters, mini-waves, persistent whole-cell waves, and oscillations. Models of different temporal and spatial scales have been developed to investigate these dynamics. Due to the complexities of the CRU network and the spatiotemporal Ca dynamics, it is challenging to model the Ca cycling dynamics in the cardiac system, particularly at the tissue scale. In this article, we review the progress of modeling of Ca cycling in cardiac systems from single RyRs to the tissue scale, the pros and cons of the current models and different modeling approaches, and the challenges to be tackled in the future.



Citation: Qu, Z.; Yan, D.; Song, Z. Modeling Calcium Cycling in the Heart: Progress, Pitfalls, and Challenges. *Biomolecules* **2022**, *12*, 1686. <https://doi.org/10.3390/biom12111686>

Academic Editors: Aman Ullah and Mohsin Saleet Jafri

Received: 10 October 2022

Accepted: 11 November 2022

Published: 14 November 2022

Publisher's Note: MDPI stays neutral with regard to jurisdictional claims in published maps and institutional affiliations.



Copyright: © 2022 by the authors. Licensee MDPI, Basel, Switzerland. This article is an open access article distributed under the terms and conditions of the Creative Commons Attribution (CC BY) license (<https://creativecommons.org/licenses/by/4.0/>).

Keywords: calcium cycling; excitation–contraction coupling; arrhythmias; computer modeling

1. Introduction

The heart is probably the most intensively and accurately modeled biological system compared to other organs [1–5]. So far, more than 100 action potential models (or modified versions) have been developed for different types of myocytes and species. Tissue and organ scale models, including one-dimensional (1D) cable, two-dimensional (2D) sheet, three-dimensional (3D) slab, and anatomically based ventricle and atrium models, have been developed. These mathematical and computational models have been widely used to investigate cardiac excitation–contraction coupling and arrhythmias under physiological and pathophysiological conditions.

Modeling of the voltage in the heart is relatively well executed, mainly following the Hodgkin–Huxley (HH) modeling approach [6]. The governing equation for the transmembrane potential (V) of a myocyte is simply described by the following differential equation: $\frac{dV}{dt} = -I_{ion}/C_m$, in which I_{ion} is the total ionic current density and C_m is the cell membrane capacitance. In cardiac myocytes, there are many types of ionic currents (Figure 1A) which are modeled either using the HH formulation or Markovian approaches. In the HH formulation, the ionic current density is described as $I_s = G_s x^m y^n z^k (V - E_s)$, in which G_s is the maximum conductance, and E_s is the reversal potential. x , y , and z are the gating variables described by differential equations with properties (steady states and time constants) from experimental measurements of whole-cell voltage clamp recordings [6]. In the Markovian approaches, there are two ways of modeling. In the first way, single ion channel openings and closings are simulated using stochastic Markovian transitions, and

the total ionic current of an assembly of ion channels is described as $I_s = g_s N_o (V - E_s)$, in which g_s is the single-channel conductance and N_o is the number of open channels at a given time. In the second way, differential equations are used to describe the probabilities of states in the Markovian scheme, and the ionic current of an assembly of ion channels is described as $I_s = G_s P_o (V - E_s)$, in which P_o is the open probability of the ion channels. Note that a ventricular myocyte is a 3D entity with its dimension being roughly [7] $150 \times 30 \times 15 \mu\text{m}^3$, but in the current action potential models, voltage is considered uniform over the entire cell membrane. In other words, at any moment, the ion channels in the entire cell membrane are assumed to sense the same voltage. Moreover, in the Markovian scheme, it is assumed that the ion channels are statistically independent, and thus the whole-cell current is simply the summation of the single-channel currents.

However, Ca cycling and its dynamics are much more complex to model. Ca cycling not only is required for contraction but also plays important roles in regulating ionic currents (Figure 1A). Ca is stored in the sarcoplasmic reticulum (SR), which forms a complex network inside the cell. Ca is released from the SR into the cytoplasmic space through the opening of the ryanodine receptors (RyRs) in the SR membrane. Opening of the RyRs is activated by Ca on both the cytoplasmic and luminal sides. Under the normal condition, SR Ca release is mainly triggered by Ca entry from the L-type Ca channels (LCCs). Under diseased or Ca overload conditions, spontaneous Ca release occur more frequently. In cardiac myocytes, RyRs form clusters (Figure 1B), which combine with their associated LCC clusters to form basic units of Ca signaling, called Ca release units (CRUs). A cell contains hundreds to thousands of CRUs [8–10], which form a coupled network via Ca diffusion in the cytoplasmic space and SR. A rich spectrum of spatiotemporal Ca dynamics is observed in cardiac myocytes and other cell types, including Ca sparks, waves, and oscillations [11–21]. Due to the complex spatiotemporal Ca dynamics, it has been challenging to model Ca cycling dynamics in the cardiac system, particularly at the tissue scales. Models of different temporal and spatial scales have been developed to investigate these spatiotemporal dynamics. In this article, we review the progress of modeling of Ca cycling in cardiac systems from single RyRs to tissue scales, the pros and cons of the current models and different modeling approaches, and the challenges to be tackled in the future.

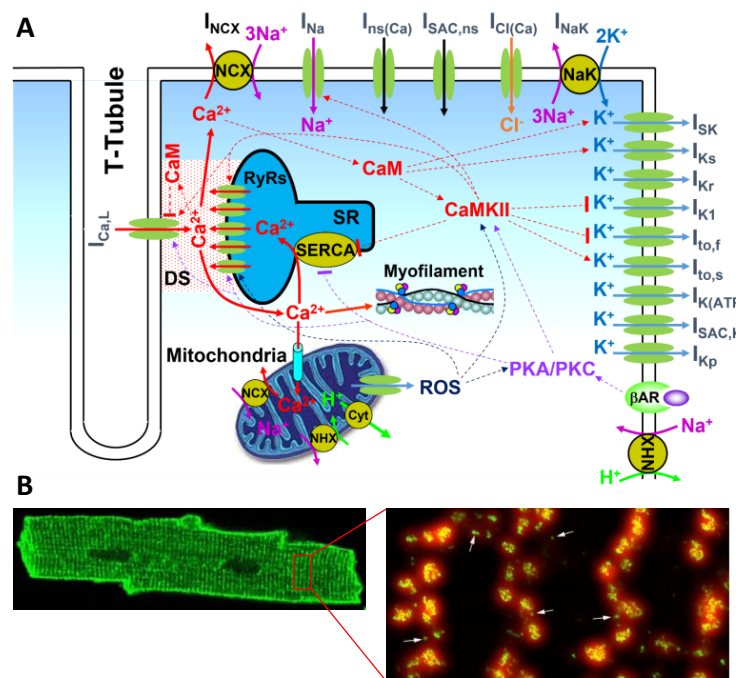


Figure 1. Ca cycling/signaling in cardiac myocytes. (A) Schematic diagram showing Ca cycling and signaling and its coupling with voltage, including the major components: (1) ionic currents and their

regulation by Ca/calmodulin (CaM) and Ca/calmodulin-dependent protein kinase II (CaMKII); (2) SR Ca release and uptake and their regulation by CaMKII and protein kinase A and C (PKA and PKC); (3) mitochondrial Ca cycling; (4) Ca and myofilament interaction; and (5) Ca-dependent signaling pathways. DS stands for dyadic space and ROS for reactive oxygen species. For a detailed explanation of each component in the diagram, see Ref. [22]. (B) RyR clusters measured from a ventricular myocyte, adapted from Ref. [9].

2. RyR Models

The RyRs are regulated by Ca from both the luminal and the cytosolic sides of SR [23–25], and thus they are sensitive to both cytosolic and SR Ca. There are several RyR models developed and used in modeling cardiac Ca cycling. The simplest model is a two-state model consisting of a closed state and an open state (Figure 2A), used in many previous simulation studies [26–28]. The close-to-open transition rate is a function of cytosolic Ca. SR Ca dependence is also added to model the luminal Ca sensitivity. A key issue that has been investigated related to RyR models is how a Ca spark is terminated spontaneously [26,27,29–34], and several mechanisms have been proposed based on computer simulations. In the scenario of the two-state model, for a Ca spark to terminate, the SR Ca content needs to be depleted to a very low level (~90% depletion) to allow the RyRs to transition from the open state to the closed state. This requires a long enough time delay between the junctional SR (JSR) and the network SR (NSR). This delay is assumed to be caused by either slow SR Ca diffusion or complex NSR structures [26,27,32]. However, this assumption is not supported by experiments which show that Ca diffusion between JSR and NSR is very fast and the JSR Ca is only depleted by around 40% (Figure 2D) [35–37]. Stern et al. [29,38] developed a four-state model which includes inactivation and recovery states (Figure 2B), in which both activation and inactivation of the RyRs are mediated by Ca in the cytosolic space. However, there is no experimental evidence that the inactivation of RyRs is mediated by cytosolic Ca. It seems that this RyR model still requires a substantial SR Ca depletion for termination of Ca sparks [31]. Shannon and Bers [39] modified the Stern et al. model by replacing cytosolic Ca-dependent inactivation with SR Ca-dependent inactivation, which allows spark termination at a much higher SR Ca level [34]. This model also allows luminal SR Ca activation of the RyRs. Restrepo et al. [40] developed a model in which inactivation is mediated by calsequestrin in the SR (Figure 2C). Other RyR models have also been developed [29,30,41–43], and the effects of RyR cooperativity are investigated [26,43–47].

Despite the effects of RyR activation and inactivation properties on spark termination, no matter how the RyRs are activated and inactivated, there is a common dynamical mechanism of spark firing and termination [31,34], in which the firing and termination of a spark are governed by a bistable switch (Figure 2E). Namely, the cytosolic Ca concentration ($[Ca]_i$) has two stable states in a range of SR Ca concentration ($[Ca]_{SR}$) (gray region in Figure 2E). When $[Ca]_i$ is at the low state, as $[Ca]_{SR}$ reaches a threshold (red arrow), spontaneous firing occurs, and $[Ca]_i$ increases to the high state. If SR depletion is fast enough to be below another threshold (cyan arrow), $[Ca]_i$ quickly switches to the low state, terminating the firing and resulting in a normal Ca spark. However, if the SR depletion cannot be low enough to reach the threshold, $[Ca]_i$ will stay at the high state, failing to terminate the spark promptly. The bistability is a result of the positive feedback due to Ca-induced Ca release. Whether there is RyR inactivation or not, $[Ca]_{SR}$ is the key parameter for the termination of sparks. For the RyR models without inactivation or weak inactivation, once SR Ca is low enough, the Ca flux from the JSR to the dyadic space is so small that $[Ca]_i$ in the dyadic space becomes low. The low $[Ca]_i$ causes the transition from the open state to the closed state to over compete the transition from the closed state to the open state, shutting off the RyRs. For the models with RyR inactivation, particularly with SR Ca-dependent inactivation, inactivation is the primary cause for shutting off the RyRs. The difference is that the termination threshold of $[Ca]_{SR}$ is much lower for the RyR models without inactivation.

When $[Ca]_{SR}$ is higher than the termination threshold, the spark can still terminate due to stochastic fluctuation of RyR openings, resulting in the so-called long-lasting sparks [31,34,48,49]. This random transition is widely known as the Kramers escape process in stochastic nonlinear systems. In other words, noise can cause the system to cross the potential barrier (the unstable state, dashed line in Figure 2E) to reach the low state. Theoretical analysis by Song et al. [34] showed that the duration of the long-lasting sparks exhibits an exponential distribution, which is described by the Kramers rate theory. Exponential distributions of spark duration have been observed in cardiac myocyte experiments in which long-lasting sparks were promoted by FK506 [48]. Note that the same random transition applies to spark firings when $[Ca]_{SR}$ is lower than the firing threshold, i.e., random fluctuations can cause transition from the low state to the high state even when $[Ca]_{SR}$ is lower than the firing threshold, following the same Kramers transition process. For LCC-triggered sparks, $[Ca]_{SR}$ is lower than the firing threshold, and Ca from the LCCs elevates $[Ca]_i$ to cross the barrier (the unstable state) to reach the high state, firing the spark. Therefore, whether the sparks are spontaneous or triggered by L-type Ca current ($I_{Ca,L}$), they follow the same dynamical mechanism.

Besides the spark dynamics, not surprisingly, how RyRs are activated and inactivated is also important for the cell-scale Ca dynamics, such as Ca alternans and Ca waves. For example, it is shown that RyR refractoriness is important for the formation of Ca alternans [50–55], indicating that the models with inactivation and refractoriness are more appropriate to describe the RyRs. Ca waves and oscillations are another widely observed phenomenon in the cardiac myocytes [17,56–59], and RyR refractoriness plays an important role in forming waves and oscillations. For example, removing the calsequestrin-mediated inactivation from the RyR model in Figure 2C, Ca waves become fractionated and irregular, as shown in simulations using a 3D cell model (Figure 2F). The simulation result agrees with the experimental observation that the R33Q mutation causes high-frequency but fractionated Ca waves (Figure 2G) [60], in which the R33Q mutation lacks the calsequestrin-mediated inactivation of RyRs. This implies that the two-state RyR model may not be appropriate for normal Ca cycling. Future modeling is needed to investigate how different RyR models affect the Ca alternans and Ca wave dynamics and compare them with experimental observations to further reveal the RyR models' appropriateness.

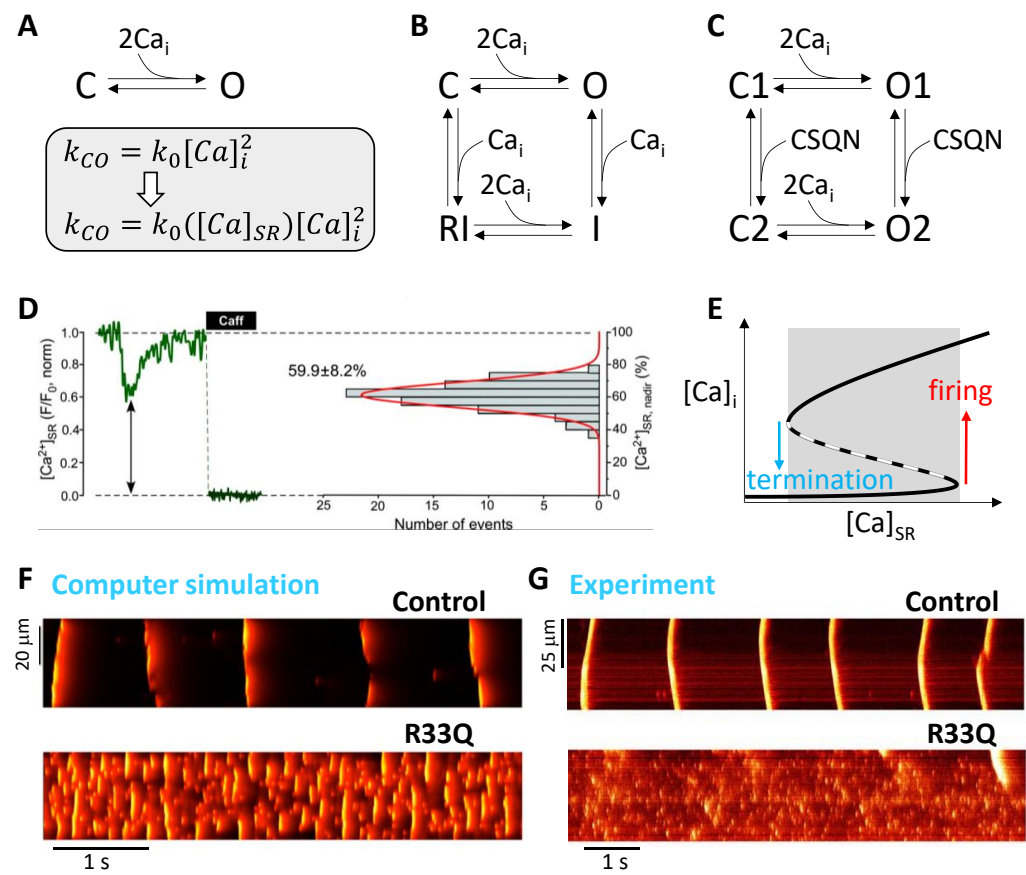


Figure 2. RyR models and Ca cycling dynamics. (A) A two-state model. The rate constant from C to O (k_{CO}) as a function cytosolic Ca without or with luminal SR Ca regulation. (B) A four-state model with cytosolic Ca-dependent inactivation developed by Stern et al. [29,38]. (C) A four-state model with calsequestrin-dependent inactivation developed by Restrepo et al. [40]. (D) Left: SR Ca during a spark and after caffeine. Right: SR Ca nadir distribution measured during sparks. Data from Zima et al. [36]. (E) Bistable switch for spark firing and termination. Red arrow marks the SR Ca threshold for spark firing and cyan arrow marks the SR Ca threshold for spark termination. Gray marks the bistable region in which the high state and low state are stable and the middle one (dashed) is unstable. (F) Upper: Time-space plots of Ca from a computer simulation of a 3D cell with the RyR model in C. Lower: Time-space plots of Ca from a computer simulation of the same 3D cell with the RyR model without the CSQN-dependent inactivation, equivalent to the two-state model in A. Simulations were done under voltage clamped at -80 mV using the 3D cell model by Song et al. [59]. (G). Time-space plots of Ca from a permeabilized rat ventricular myocyte of control (upper) and R33Q mutation (lower), adapted from Ref. [60].

3. Single CRU and CRU Network Models

Models of single CRU with different spatial resolutions have been developed. In 1992, Stern [61] put forth a theory for excitation-contraction coupling to explain the graded response of Ca release to $I_{Ca,L}$, in which a local control (or “cluster bomb”) model is assumed. In this local control model, an LCC triggers a cluster of RyRs to open collectively, resulting in an all-or-none discretized release event. The all-or-none release events are probability events proportional to the strength of $I_{Ca,L}$, giving rise to the experimentally observed whole-cell graded response. This cluster bomb model can be considered as the first single CRU model. In 1993, the discretized release events, called Ca sparks, were demonstrated in experiments [21]. Later, more detailed CRU models [26,29,38,62] that include stochastic RyR openings and different compartments were developed to investigate the spark dynamics, especially the mechanism of termination of a spark as described earlier. Higher spatial resolution and more realistic CRU models were also developed,

including realistic T-tubule structure reconstructed from experiments (Figure 3A) [63], spatially distributed RyRs with Ca diffusion in the dyadic space [27,28,32,64] and complex SR network structures (Figure 3B) [27,32]. These high-resolution models provide further details on spark firing and termination properties.

To investigate the Ca cycling dynamics in a whole cell, one needs to develop a model consisting of hundreds and thousands of CRUs. It is difficult to implement the complex CRU models as in Figure 3A,B into a cell model. CRU network models [40,52,57,65–69] composed of simpler CRU models were developed. These models are used to investigate the spatiotemporal Ca cycling dynamics, including Ca alternans and Ca waves. As an example, Figure 3C shows a scheme of a CRU network model developed by Nivala et al. [57,58,66]. The model consists of a 3D network of CRUs. Each CRU contains four types of spaces, bulk myoplasm, dyadic space, junctional SR, and network SR. Unlike the CRU models in Figure 3A,B, the dyadic space is a single compartment in this model and thus there is no Ca diffusion, i.e., the RyRs in a CRU sense the same Ca in the dyadic space. The CRUs are coupled via Ca diffusion in the SR and cytoplasm. Figure 4 shows the spatiotemporal Ca cycling dynamics as extracellular Ca concentration increases in the same CRU network model as in Figure 3C [57], undergoing a phase transition with criticality [70,71]. These same sequences of dynamics were demonstrated in experiments of ventricular myocytes [57]. Most of the 3D whole-cell models are similar but differ somewhat in spatial resolution and structural details, e.g., some with structural complexities between those in Figure 3A–C (see Colman et al. for a detailed review [4]). Although the CRU network models lack the realistic structures of the TT and the SR networks as the real one in Figure 3A, or even as the complex one in Figure 3B, they are much more computationally convenient, and can be easily modified to simulate different subcellular structures, different cell types, and diseased conditions [68,72].

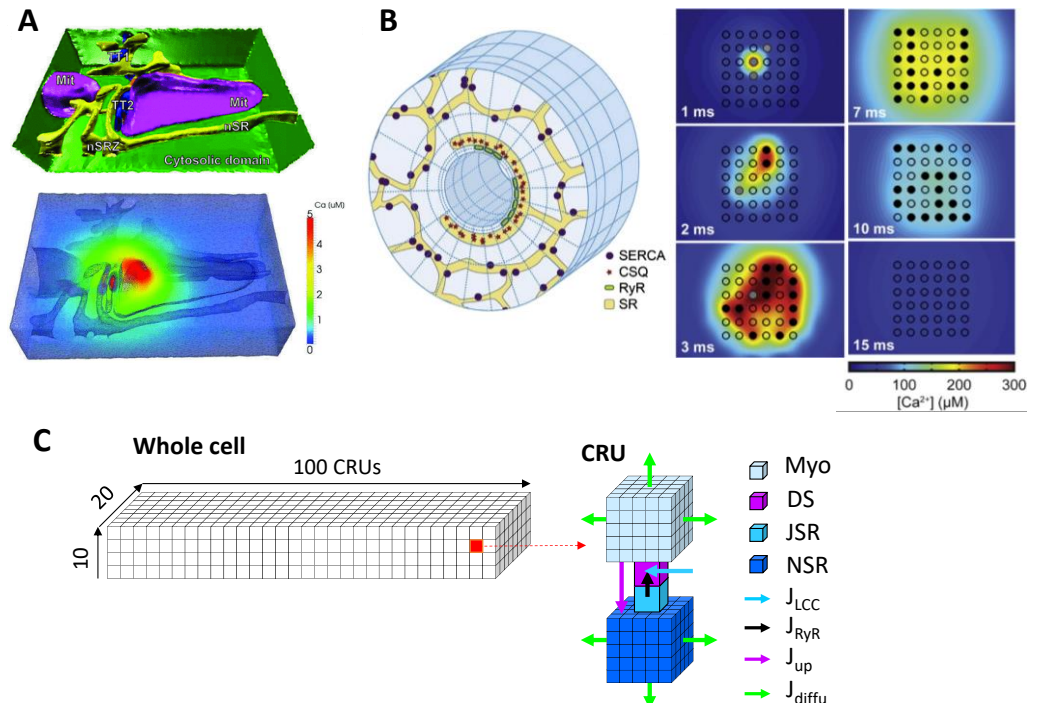


Figure 3. Single CRU and CRU network models. (A) CRU model with realistic structure, adapted with permission from Ref. [63], copyright 2012, John Wiley and Sons. Upper: Structure. Lower: A Ca snapshot during a Ca spark. (B) A detailed CRU model, adapted with permission from Ref. [32], copyright 2013, Elsevier. Left: Model structure. Right: Snapshots of Ca at different time points in the dyadic space. (C) A CRU network model to represent the whole cell [57,66]. Left: A 3D network consisting of $100 \times 20 \times 10$ CRUs, representing a whole cell. Right: Structure of a CRU. Colored cubes mark different spaces and arrows indicate different fluxes.

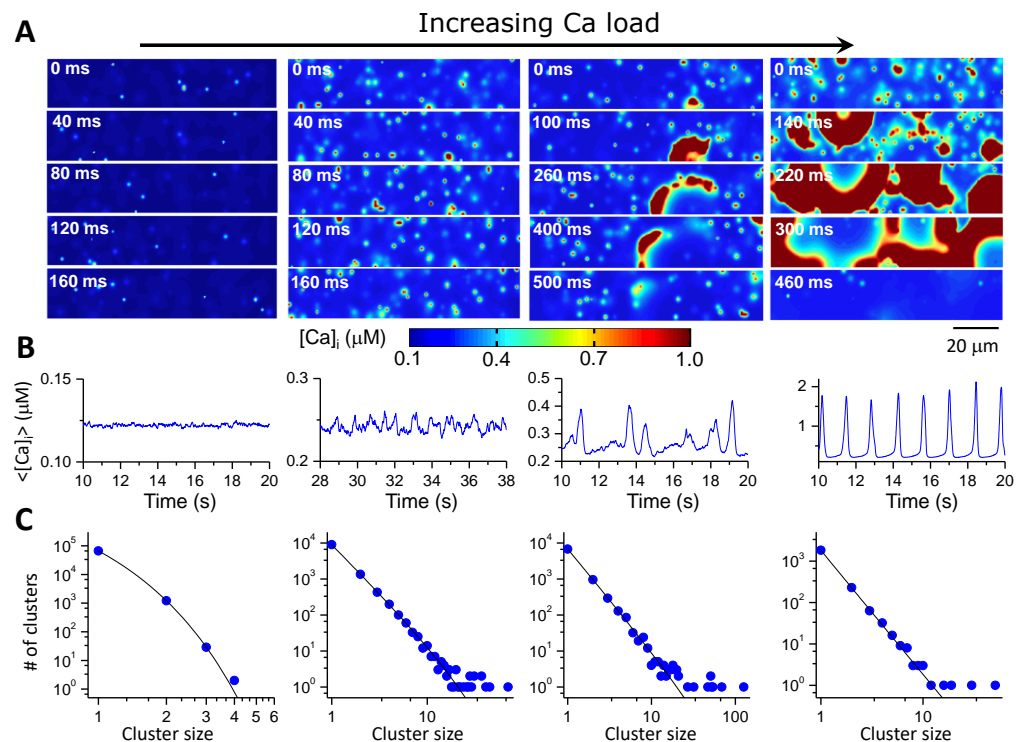


Figure 4. Spatiotemporal Ca cycling dynamics in a 3D CRU network model [57]. (A) Snapshots of Ca concentration in the cytoplasmic space for different Ca loading achieved by altering extracellular $[Ca]_o$. From left to right, $[Ca]_o = 3$ mM, 9 mM, 10 mM, and 16 mM. (B) Averaged whole-cell Ca concentration for the corresponding loading conditions. (C) Number of clusters versus spark cluster size. Symbols are data from simulations and lines are reference lines. The line in the left most panel is exponential, but those in other panels are linear, indicating power-law distribution. Power-law clustering indicates that a critical phenomenon [70,71] occurs during the transition from individual sparks to waves. Adapted with permission from Ref. [57], copyright 2012, Elsevier.

4. Modeling SR Ca Cycling in Single-Cell Action Potential Models

In early action potential models, such as the Noble model [73], the Beeler–Reuter model [74], and the 1991 Luo and Rudy model [75], there is no or trivial intracellular Ca cycling. Ca cycling was added in the later action potential models using different modeling approaches.

Global RyR models. In this type of models, one assumes that SR Ca release is uniform in the whole cell, and thus uses a single-channel RyR model to describe the whole-cell SR Ca release. We call this type of Ca release models as global RyR models. The first action potential model with intracellular Ca cycling is the DiFrancesco–Noble model for sinoatrial nodal (SAN) cells [76], in which Ca-induced Ca release based on Fabiato’s theory [77] was implemented with the SR Ca release flux (we denoted it as J_{rel} in this paper) being formulated as: $J_{rel} = \alpha_{rel}[Ca]_{rel} \frac{[Ca]_i^2}{[Ca]_i^2 + K_{m,Ca}}$. This formulation is equivalent to the two-state RyR model in Figure 2A. This Ca cycling model was modified for excitation-contraction coupling in a rabbit atrial cell model [78]. Jafri et al. [79] developed an action potential model with Ca cycling by adopting the Keizer and Levine’s RyR model [41] for SR Ca release, and Shannon and Bers [39] developed an action potential model by using a modified Stern et al. RyR model (Figure 2B), in which SR Ca-dependent activation was added and SR Ca-dependent inactivation was used. The RyR model by Shannon and Bers was also adopted by Maltsev and Lakatta for their SAN cell model [80]. In these models, J_{rel} is formulated as $J_{rel} = kP_o([Ca]_{SR} - [Ca]_i)$ in which P_o is the open probability calculated from the RyR model. Since in this type of models, the whole cell contains a single cytosolic Ca pool and a single SR Ca pool, and thus all the RyRs in whole cell sense the same cytosolic Ca and

the same SR Ca. These models are called “common-pool” models. However, as pointed out by Stern [61], the “local-control” model is more appropriate for $I_{Ca,L}$ triggered SR Ca release exhibiting graded response. On the other hand, the common-pool model with a global RyR model allows spontaneous Ca release responsible for delayed afterdepolarizations (DADs) in ventricular cells [81] or the Ca clock in SAN cells [80].

Phenomenological SR Ca release models. In many of the action potential models, instead of using a RyR model, SR Ca release is modeled phenomenologically. For example, in the 1994 Luo and Rudy model [82,83], J_{rel} was modeled as: $J_{rel} = G_{rel}([Ca]_{SR} - [Ca]_i)$ with $G_{rel} \propto f(\Delta Ca_{i,2}) \left[1 - \exp\left(-\frac{t}{\tau_{on}}\right)\right] \exp\left(-\frac{t}{\tau_{off}}\right)$. $\Delta Ca_{i,2}$ is the Ca change at 2 ms after \dot{V}_{max} , and if this change is below the given threshold, $G_{rel} = 0$. Since $\Delta Ca_{i,2}$ is caused by Ca entry from LCCs, thus G_{rel} is $I_{Ca,L}$ -dependent. Another type of phenomenological Ca release model [84–88] uses the following type of formulation for J_{rel} : $J_{rel} = G_{rel}xy([Ca]_{SR} - [Ca]_i)$, in which x and y are activation and inactivation gating variables formulated in the form of HH formulism as for the membrane ionic currents. In this type of model, the activation gating x 's steady state (x_{∞}) is a function of $I_{Ca,L}$, and thus Ca release is $I_{Ca,L}$ -dependent. In a study by Livshitz and Rudy [89], they used a Ca release model by the following differential equation of J_{rel} : $\frac{dJ_{rel}}{dt} = -\frac{J_{rel,\infty} + J_{rel}}{\tau_{rel}}$, in which $J_{rel,\infty}$ is a function of $I_{Ca,L}$ and SR Ca. This formulation was later adopted in the human model by O'Hara et al. [90]. The authors stated that they developed a two-state (closed-open) model of SR Ca release, but it is unclear how a differential equation for J_{rel} can be derived from the two-state model. On the other hand, a similar equation was derived earlier by Shiferaw et al. [91] based on spark statistics (see below). Note that in these models, SR Ca release is a function of $I_{Ca,L}$, i.e., SR Ca release is triggered by $I_{Ca,L}$, which can effectively model the graded response of Ca release. However, if $I_{Ca,L} = 0$, no SR Ca release can occur in these models, indicating that spontaneous Ca release cannot be appropriately modeled. On the other hand, these models can exhibit Ca alternans [84–86,89]. As will be discussed below, a phenomenological spontaneous release term can be added to these models for modeling spontaneous Ca release.

Spark statistics-based models. Shiferaw et al. [91] took a different approach to develop an SR Ca release model based on spark dynamics and statistics, which was improved in the Mahajan et al. model [92]. The basic idea is that Ca sparks are triggered by $I_{Ca,L}$ and the rate of spark generation is proportional to $I_{Ca,L}$, i.e., $\frac{dN}{dt} \propto I_{Ca,L}$. On the other hand, a Ca spark has a limited lifetime, and Ca sparks disappear over time. By considering the spark birth-and-death process, they derived a differential equation for J_{rel} as [92]: $\frac{dJ_{rel}}{dt} = N(I_{Ca,L})Q(c_{JSR})c_{JSR} - \frac{J_{rel}}{T}$, in which $N(I_{Ca,L})$ is the number of sparks as a function of $I_{Ca,L}$, T is a time constant related to the spark lifetime, $Q(c_{JSR})$ is the fractional SR Ca release which can be experimentally determined [93,94]. Similar to the phenomenological models, this model cannot exhibit spontaneous Ca release but can exhibit Ca alternans. Indeed, this model is the first to reveal the role of fractional Ca release in the genesis of Ca alternans.

Local-control models. In 2002, an action potential model with a local-control model of Ca cycling was developed by Greenstein and Winslow [42]. In this model, thousands of CRUs with stochastic RyRs and LCCs are implemented with a common bulk cytosolic space. A simpler version was developed later [95]. Similar local-control models were developed and simulated with advanced numerical methods and mathematical approaches to speed up computation [96,97]. As expected, these models can well simulate the graded response. Moreover, it can exhibit Ca alternans [98]. Although no studies have been carried out to show spontaneous Ca release in these models, in principle, this type of model is capable of simulating spontaneous Ca release to result in Ca oscillations. A caveat of this type of model is that the Ca released from the SR enters into the common bulk cytosolic space, lacking the capability for spatiotemporal Ca cycling dynamics. Since it contains CRUs in the order of 10,000, it is computationally nontrivial and difficult to be used for tissue-scale simulations.

Spatially extended cell models. More recently, action potential models containing a 3D CRU network for Ca cycling have been developed to investigate Ca cycling dynamics

and their coupling with voltage [40,52,57,66–68]. These models are truly local control models which can exhibit the whole spectrum of spatiotemporal Ca cycling dynamics (e.g., Figure 4). These models can be easily adapted for different types of cells, such as atrial myocytes [99–103] and SAN cells [104,105] that exhibit complex T-tubular structures [106,107], as well as subcellular structural remodeling in heart failure [72] in which T-tubule disruption occurs [108–110]. Other action potential models with spatially extended Ca cycling have also been developed to simulate subcellular Ca alternans and triggered activities [46,111–115]. A major caveat is that the spatially extended models are computationally challenging to use for tissue-scale simulations.

As mentioned above, each type of model has its advantages and pitfalls. A common issue of the non-spatial models is that they cannot properly simulate DADs. Even if some of them can simulate DADs, such as the model by Shannon and Bers [81], it cannot capture the stochastic nature of DADs [59,116–118] as well as the positive feedback between voltage and Ca releases that give rise to the dynamics of the triggered activity [59,116]. As shown in Figure 4, when intracellular Ca is low, such as under normal conditions, the Ca sparks are independent stochastic events (i.e., no spark-induced sparks). Thus, a statistical approach used by Shiferaw et al. [91] to derive the Ca release equation is a more rigorous approach (i.e., the differential equation is derived based on first principles) than others. Therefore, the model by Shiferaw et al. is more appropriate for the condition of low or normal Ca level. On the other hand, when Ca is very high, Ca oscillates synchronously and almost periodically; the global RyR modeling approach is more appropriate. However, none of the models (except for the spatial cell models) can correctly capture the dynamics at the intermediate range of Ca level where large random fluctuations occur due to criticality (Figure 4). This is the range where DADs and triggered activity occur.

Besides DADs, it has been shown experimentally that early afterdepolarizations (EADs), although mainly caused by reactivation of $I_{Ca,L}$ [119], can also be caused by spontaneous Ca release [120–123]. Spatially extended 3D cell models [124,125] have been used to investigate the roles of spontaneous Ca release in the genesis of EADs, which can capture certain features of the experimental observations. Wilson et al. [126] modified a non-spatial cell model, the Shannon and Bers model [39], to exhibit spontaneous Ca oscillation and investigated spontaneous Ca release/oscillation on EAD genesis. However, in this model, the voltage depolarizations for EADs occur much earlier than the corresponding spontaneous Ca releases (the Ca oscillation and the voltage oscillation for EADs are almost in opposite phase) [126,127], which does not agree with the experimental observation that the rise of Ca occurs slightly ahead of the voltage depolarization of an EAD (experimental evidence to support that Ca release causes the EAD, not the other way around) [122,123]. Due to the spatiotemporal nature of the Ca cycling dynamics, the same problems remain for modeling spontaneous Ca release induced EADs as those for modeling DADs using the non-spatial action potential models.

5. Modeling Mitochondrial Ca Cycling and Energetics in Action Potential Models

Mitochondria are not only the energy store but also another Ca store for the cell (Figure 1A) and play important roles in intracellular Ca cycling and cardiac function [128,129]. Mitochondrial metabolism provides energy for ion pumps, including Na-Ca exchanger, Na-K pump, and SERCA pump. Furthermore, there are ATP-sensitive K channels and RyRs are also regulated by ATP. Besides providing energy for the ion channels and pumps, mitochondria also participate directly in intracellular Ca cycling. Cytosolic Ca enters into mitochondria via mitochondrial Ca uniporter and extrudes from mitochondria via mitochondrial Na-Ca exchanger. Ca may also get out of mitochondria via the transient opening of the mitochondrial permeability transition pore. Non-spatial (single mitochondrial compartment) models integrating mitochondrial metabolism and Ca cycling have been developed to simulate the effects of mitochondria on Ca cycling and arrhythmogenesis [130–134]. However, mitochondria form a network inside the cell, which can exhibit complex spatiotemporal mitochondrial depolarization dynamics, such as critical phenomenon in mitochondrial

depolarization [135,136]. In our recent publications [137–140], we developed a model with a spatially distributed mitochondrial network and used it to investigate Ca alternans, EADs, and spontaneous Ca release induced DADs and triggered activity. Similar to the case without mitochondria in the model, when Ca dynamics becomes spatiotemporal, the single mitochondrial compartment model may fail to capture the Ca cycling dynamics and network models are needed.

6. Modeling Ca-Dependent Signaling

Ca-dependent signaling (Figure 1A) plays key roles in cardiac excitation-contraction coupling and arrhythmogenesis [22,141]. Pathways of β -adrenergic signaling, protein kinase A/C signaling, reactive oxygen species-dependent signaling, and Ca/calmodulin-dependent protein kinase II signaling have been incorporated into many action potential models [87,90,138,142–146], which have been used to investigate their effects on action potential and Ca cycling dynamics. Most of the models are non-spatial models, and it has not been investigated how the complex spatiotemporal Ca cycling dynamics will affect the Ca-dependent signaling which then affects the Ca cycling and action potential dynamics.

7. Tissue-Scale Modeling for Spatiotemporal Ca and Voltage Dynamics

In most of the tissue-scale simulations, non-spatial cell models were used. As mentioned above, these models cannot properly model DADs and DAD-mediated triggered activities as well as spontaneous Ca release mediated EADs. To simulate the effects of spontaneous Ca release on arrhythmias at the tissue scale, different approaches have been used. A simple and straightforward way of modeling was used [118,147], in which stochastic DADs were phenomenologically implemented by commanding stochastic SR Ca release with statistical properties from experimental data. Chudin et al. [84] added phenomenologically a spontaneous release term to the release flux as: $J_{spon} = kP_{spon}([Ca]_{SR} - [Ca]_i)$, in which P_{spon} , described by a differential equation, is a gating variable depending on cytosolic Ca. Chen and Shiferaw [111] developed a phenomenological model by adding a spontaneous spark generation term $R_{SCR}(t)$ to the differential equation for J_{rel} and used a small 1D array to calculate $R_{SCR}(t)$. This model was used in a whole-heart simulation for random DADs and triggered arrhythmias [111,148]. Colman et al. [149,150] developed a multi-scale modeling approach in which a phenomenological spontaneous release function was derived based on the detailed 3D single-cell simulations, and used it to simulate DAD-mediated arrhythmias in tissue models. More recently, a phenomenological model for Ca wave induced APD alternans in atrial cells was developed and used in atrial tissue for alternans induced arrhythmias [99,151]. Walker et al. [152] simulated a 100-cell cable with a detailed 3D cell model and developed a spatial-average filtering method for estimating the probability of extreme stochastic events from a limited set of spontaneous Ca^{2+} release profiles to predict DAD events in tissue.

Although these simulation studies have provided useful information and mechanistic insights into DAD-mediated arrhythmias, they have their pitfalls. One major issue is the effects of the feedback between Ca and voltage when complex spatiotemporal dynamics occurs. This feedback is lacking in the current multi-scale modeling approaches. Moreover, tissue simulations with detailed 3D cell models are needed to validate the results of the phenomenological models, however, this is computationally non-trivial for large tissue sizes.

We recently developed a parallel computational method using multiple graphics processing unit (GPU) cards, which allows us to simulate large tissue sizes with a 3D cell model. Figure 5 shows one of our simulations (unpublished data) in which a DAD occurs after a pacing beat in a 100×100 -cell tissue using a detailed 3D cell model that is the same as in Song et al. [59]. Figure 5A shows the voltages and whole-cell Ca transients from a line of 100 cells in the tissue. Figure 5B shows Ca snapshots from the surface of the entire 100×100 -cell tissue at three different time points as marked. Figure 5C,D show zoom-in views of Ca snapshots from a 20×20 -cell area (Figure 5C) and a 3×3 -cell area (Figure 5D).

As shown in Figure 5D, during the DAD, the Ca waves occur in the cells, and the waves are randomly different from cell to cell.

In the simulations shown in Figure 5, the 3D cell model contains $100 \times 20 \times 10$ CRUs, and thus the tissue contains a total of 2×10^8 CRUs. Since each CRU has 100 RyRs and 10 LCCs, thus the tissue contains 2×10^{10} RyRs and 2×10^9 LCCs. The RyRs are described by a four-state Markovian model (Figure 2C) and the LCCs are described by a seven-state Markovian model. The simulation was carried out on 10 Nvidia GTX 3090 cards using ~ 41.5 GiB GPU memory in total. The time step for the simulation was 0.01 ms. It costs ~ 3.5 computational hours to compute 1 s of the model time. Of note, our method is computationally scalable, meaning that we can perform larger tissue-size simulations with more available GPU cards within a reasonable computational run time.

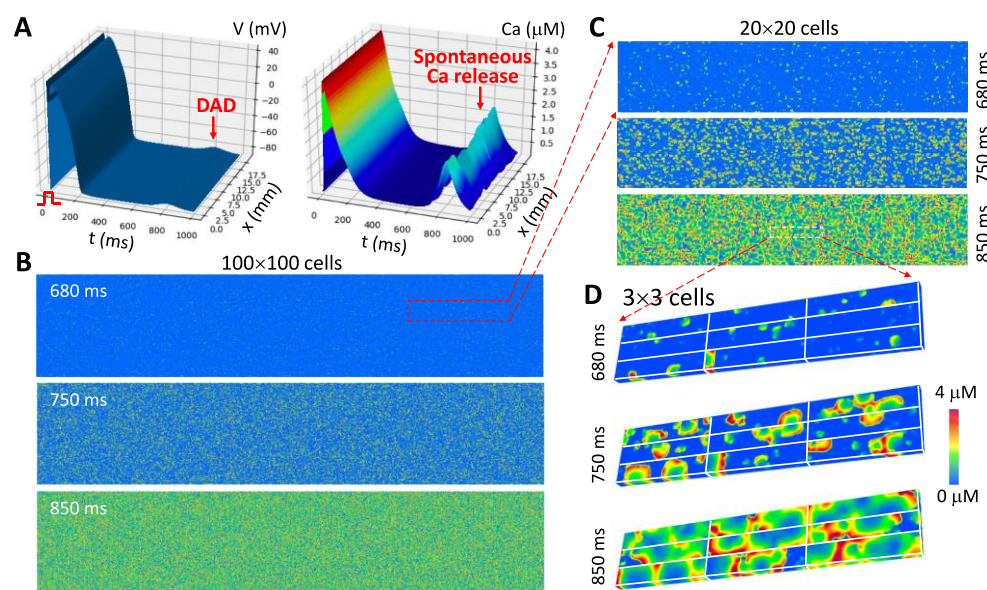


Figure 5. Computer simulation of a 100×100 -cell 2D tissue using a 3D spatial cell model showing spontaneous Ca release and DAD following a paced beat. (A). Voltage (left) and whole-cell Ca transient (right) from a line of 100 cells in the tissue. The action potential was elicited by a stimulus applied at $t = 0$. (B). Ca snapshots (recorded on the surfaces of the 3D cells) in the 100×100 -cell tissue taken from three time points as marked. (C). A zoom-in view of Ca snapshots from a small area (20×20 cells) for the three time points. (D). A zoom-in view of Ca snapshots from an even smaller area (3×3 cells) showing stochastic Ca wave dynamics inside the cells. Plotted is a 3D surface view of Ca on the surface of the 9 cells. The 3D cell model consist of $100 \times 20 \times 10$ CRUs and the cell model is the same as in Song et al. [59]. The tissue model contains 2×10^{10} RyRs (four-state model in Figure 2C) and 2×10^9 LCCs, both are simulated with stochastic Markovian transitions. The time step for the simulation is $\Delta t = 0.01$.

8. Challenges for Future Modeling

Despite the progress in modeling Ca cycling at different scales in the heart, there are still plenty of challenges. A general problem is how to develop low-dimensional models or multi-scale modeling approaches to link the dynamics from the protein scale to the whole heart. Several gaps need to be filled:

- (1) The first gap is to simulate sparks from a high spatial resolution CRU model to a non-spatial CRU model. As shown in the high spatial resolution models [27,28,32] (see also Figure 3B), Ca spark dynamics are spatiotemporal and depend on the spatial distribution of the RyRs in the dyadic space. Moreover, Maltsev et al. [64] showed that the occurrence of Ca sparks harnesses the Ising phase transition in a 2D array of RyRs. On the other hand, the majority of the single CRU and CRU network models ignore these spatiotemporal properties by using a RyR cluster without spatial placement

of RyRs. How to correctly capture the properties of the phase transition and large fluctuations of the spatiotemporal system using a lower-resolution or non-spatial model needs to be investigated.

- (2) The second gap is from CRUs (sparks) to a low-dimensional whole-cell model (Ca waves and whole-cell Ca transient). So far, using the 3D cell model for large tissue and whole-heart simulations is computationally nontrivial. Low-dimensional representations of the cell are preferred. As shown extensively by experiments and simulations (e.g., Figure 4), there is a hierarchy of Ca dynamics: quarks, sparks, spark clusters, mini-waves, persistent waves, and whole-cell oscillations. How to develop a low-dimensional model to embrace these dynamics is a nontrivial challenge. As mentioned above, when Ca is low or normal, the differential equation describing the SR Ca release by Shiferaw et al. is a correct approach. At very high Ca where SR Ca release is synchronous, the global RyR model is appropriate. However, neither of the two modeling approaches can capture the Ca dynamics in the intermediate Ca range. As shown in Figure 4 (see Nivala et al. [57]), a second-order phase transition occurs for the transition from independent individual spark dynamics to the whole-cell oscillations, i.e., a critical phenomenon exists. How to model the dynamics at this phase transition using a low-dimensional representation is unknown since when criticality occurs, the dynamics is intrinsically high-dimensional. Another challenge is how to model complex 3D T-tubular structures in low-dimensional models. For example, T-tubules are disrupted in failing ventricular myocytes [108–110], which can cause nontrivial changes in both Ca cycling and action potential dynamics [68,72]. Correctly modeling these effects is essential for tissue-scale modeling of heart failure. Furthermore, when Ca cycling dynamics becomes spatiotemporal, their effects on Ca-dependent ionic currents and signaling, such as $I_{Ca,L}$ and I_{NCX} as well as Ca-activated potassium currents (Figure 1A), and thus on the action potential dynamics may be nontrivial [125]. How to model these effects using a low-dimensional model is another issue needed to be concerned.
- (3) The third gap is from a single cell to a syncytium (tissue and whole heart). For tissue or whole-heart simulations, cardiac tissue is treated as a syncytium with discretization in computer simulations being typically from $\Delta x = \Delta y = \Delta z = 0.1$ to 0.5 mm [3,153–155]. The dimension of a typical myocyte is $0.15 \times 0.03 \times 0.015$ mm³, which indicates that one “computational cell” is equivalent to 15 to 1500 real cells. Under normal conditions in which conduction is fast and Ca is mainly determined by $I_{Ca,L}$ (so that Ca is synchronized by $I_{Ca,L}$ in different cells), this type of discretization is appropriate. However, under diseased conditions, such as ischemia and heart failure, cells are weakly coupled and the Na current is attenuated, and thus the action potential conduction in tissue is slow. For slow conduction, a discretization at the cell size is more appropriate [156,157]. Moreover, when spatiotemporal Ca dynamics, such as waves and alternans, occur in the cell, these dynamics may be dyssynchronous from cell to cell [158] (see Figure 5), and thus a resolution of the cell size may be required for investigating these dynamics. Large tissue or whole-heart simulations with a resolution at the cell size scale is computationally nontrivial.
- (4) Mitochondrial Ca cycling [131,137,138,159] and Ca-myofilament interactions [160,161] play important roles in Ca cycling dynamics. How to include their effects in a low-dimensional representation of a cell is also challenging.
- (5) Although stochastic Markovian models are used to simulate single ion channel dynamics, they are still phenomenological models describing the transitions of an ion channel among different hypothetical states. Molecular dynamics simulations of single ion channels at the atomic scale are more accurate representations, which can provide parameter information for transition rates of Markovian models used in cell and tissue simulations, linking the molecular scale effects of gene mutations or drugs to cellular and tissue scale behaviors [162,163]. However, molecular dynamics

simulation is computationally tedious [164], and it is still a major challenge to use it for the development and validation of Markovian models.

The central issue among these challenges is dimension reduction. Coarse graining and mean-field theories are typical modeling approaches to reduce a high-dimensional representation to a low-dimensional one [165]. Approaches for dimension reduction specific to ion channel models have been developed. For example, Fox derived a Langevin equation for a population of ion channels described by stochastic Markovian transitions for the HH formulation [166]. Keener [167] showed that many Markovian models of ion channel kinetics have globally attracting stable invariant manifolds, which can substantially simplify the computation with no approximation. He showed that this applies to certain models of potassium channels, sodium channels, and RyRs. Phenomenological modeling is currently the major modeling approach that uses low-dimensional models to describe high-dimensional systems. Iterated maps are another low-dimensional representation of high-dimensional systems [53,151,168,169]. However, both phenomenological modeling and iterated maps rely on experimental data for validation and are only valid for certain conditions.

Theoretically, if one has all the details of a system, one can build up a mathematical model to describe the motion of the atoms following Newton's laws of motion or quantum mechanics. However, it is impossible to simulate such models due to computational limitations, at least in the foreseen future. Even if one can simulate such a big system, it is still too complex to be understandable. On the other hand, a main task of science is to reduce complex systems into ones that can be grasped by the human brain and establish principles and theories which can be passed from generation to generation. Therefore, developing low-dimensional representations that can capture the dynamics or multi-scale modeling approaches that can link the dynamics at different scales is crucial for understanding complex biological systems, such as Ca cycling in the heart.

9. Conclusions

The heart is so far the most widely and accurately modeled organ, and it has the potential to use the models and simulations at bedside to guide treatments. Much progress has been made for the past several decades of cardiac modeling, including models from single proteins (ion channels), whole-cell Ca cycling and action potential models, and whole-heart models. Mathematical and computational methods, such as multiscale modeling approaches and advanced numerical algorithms, have been developed. These modeling efforts have greatly helped the understanding of cardiac excitation–contraction coupling and arrhythmogenesis. Despite the progress in the last several decades, there are still plentiful pitfalls in the current models, modeling approaches, and simulation methods. The challenges to overcome these pitfalls are nontrivial but highly worthwhile for the upcoming generation of modelers to pursue in their future careers.

Funding: This research was funded by National Institutes of Health grants R01 HL134709, R01 HL139829, R01 HL134346, and R01 HL157116 (Z.Q.), and Natural Science Foundation of China Grant No. 82172067 (Z.S.).

Institutional Review Board Statement: Not applicable.

Conflicts of Interest: The authors declare no conflict of interest.

References

1. Noble, D. Modeling the heart—from genes to cells to the whole organ. *Science* **2002**, *295*, 1678–1682. [[CrossRef](#)] [[PubMed](#)]
2. Henriquez, C.S. A Brief History of Tissue Models For Cardiac Electrophysiology. *IEEE Trans. Biomed. Eng.* **2014**, *61*, 1457–1465. [[CrossRef](#)] [[PubMed](#)]
3. Trayanova, N.A. Whole-heart modeling: Applications to cardiac electrophysiology and electromechanics. *Circ. Res.* **2011**, *108*, 113–128. [[CrossRef](#)] [[PubMed](#)]
4. Colman, M.A.; Alvarez-Lacalle, E.; Echebarria, B.; Sato, D.; Sutanto, H.; Heijman, J. Multi-scale computational modeling of spatial calcium handling from nanodomain to whole-heart: Overview and perspectives. *Front. Physiol.* **2022**, *13*, 836622. [[CrossRef](#)]

5. Qu, Z.; Hu, G.; Garfinkel, A.; Weiss, J.N. Nonlinear and stochastic dynamics in the heart. *Phys. Rep.* **2014**, *543*, 61–162. [[CrossRef](#)] [[PubMed](#)]
6. Hodgkin, A.L.; Huxley, A.F. A Quantitative Description of Membrane Current and Its Application to Conduction and Excitation in Nerve. *J. Physiol.* **1952**, *117*, 500–544. [[CrossRef](#)] [[PubMed](#)]
7. Bers, D.M. *Excitation-Contraction Coupling and Cardiac Contractile Force*, 2nd ed.; Kluwer Academic Publishers: Dordrecht, The Netherlands, 2001.
8. Soeller, C.; Crossman, D.; Gilbert, R.; Cannell, M.B. Analysis of ryanodine receptor clusters in rat and human cardiac myocytes. *Proc. Natl. Acad. Sci. USA* **2007**, *104*, 14958–14963. [[CrossRef](#)]
9. Baddeley, D.; Jayasinghe, I.D.; Lam, L.; Rossberger, S.; Cannell, M.B.; Soeller, C. Optical single-channel resolution imaging of the ryanodine receptor distribution in rat cardiac myocytes. *Proc. Natl. Acad. Sci. USA* **2009**, *106*, 22275–22280. [[CrossRef](#)]
10. Hiess, F.; Vallmitjana, A.; Wang, R.; Cheng, H.; ter Keurs, H.E.D.J.; Chen, J.; Hove-Madsen, L.; Benitez, R.; Chen, S.R.W. Distribution and Function of Cardiac Ryanodine Receptor Clusters in Live Ventricular Myocytes. *J. Biol. Chem.* **2015**, *290*, 20477–20487. [[CrossRef](#)]
11. Camacho, P.; Lechleiter, J.D. Increased frequency of calcium waves in *Xenopus laevis* oocytes that express a calcium-ATPase. *Science* **1993**, *260*, 226–229. [[CrossRef](#)]
12. Lipp, P.; Niggli, E. Microscopic spiral waves reveal positive feedback in subcellular calcium signaling. *Biophys. J.* **1993**, *65*, 2272–2276. [[CrossRef](#)]
13. Skupin, A.; Kettenmann, H.; Winkler, U.; Wartenberg, M.; Sauer, H.; Tovey, S.C.; Taylor, C.W.; Falcke, M. How does intracellular Ca^{2+} oscillate: By chance or by the clock? *Biophys. J.* **2008**, *94*, 2404–2411. [[CrossRef](#)] [[PubMed](#)]
14. Bootman, M.D.; Berridge, M.J.; Lipp, P. Cooking with calcium: The recipes for composing global signals from elementary events. *Cell* **1997**, *91*, 367–373. [[CrossRef](#)]
15. Marchant, J.S.; Parker, I. Role of elementary Ca^{2+} puffs in generating repetitive Ca^{2+} oscillations. *EMBO J.* **2001**, *20*, 65–76. [[CrossRef](#)]
16. Cheng, H.; Lederer, M.R.; Lederer, W.J.; Cannell, M.B. Calcium sparks and $[Ca^{2+}]_i$ waves in cardiac myocytes. *Am. J. Physiol.* **1996**, *270*, C148–C159. [[CrossRef](#)] [[PubMed](#)]
17. Wier, W.G.; ter Keurs, H.E.; Marban, E.; Gao, W.D.; Balke, C.W. Ca^{2+} ‘sparks’ and waves in intact ventricular muscle resolved by confocal imaging. *Circ. Res.* **1997**, *81*, 462–469. [[CrossRef](#)]
18. Lukyanenko, V.; Gyorke, S. Ca^{2+} sparks and Ca^{2+} waves in saponin-permeabilized rat ventricular myocytes. *J. Physiol.* **1999**, *521*, 575–585. [[CrossRef](#)]
19. Thurley, K.; Tovey, S.C.; Moenke, G.; Prince, V.L.; Meena, A.; Thomas, A.P.; Skupin, A.; Taylor, C.W.; Falcke, M. Reliable encoding of stimulus intensities within random sequences of intracellular Ca^{2+} spikes. *Sci. Signal* **2014**, *7*, ra59. [[CrossRef](#)]
20. Cheng, H.; Lederer, W.J. Calcium Sparks. *Physiol. Rev.* **2008**, *88*, 1491–1545. [[CrossRef](#)]
21. Cheng, H.; Lederer, W.J.; Cannell, M.B. Calcium sparks: Elementary events underlying excitation-contraction coupling in heart muscle. *Science* **1993**, *262*, 740–744. [[CrossRef](#)]
22. Qu, Z.; Weiss, J.N. Mechanisms of Ventricular Arrhythmias: From Molecular Fluctuations to Electrical Turbulence. *Annu. Rev. Physiol.* **2015**, *77*, 29–55. [[CrossRef](#)] [[PubMed](#)]
23. Jiang, D.; Wang, R.; Xiao, B.; Kong, H.; Hunt, D.J.; Choi, P.; Zhang, L.; Chen, S.R. Enhanced store overload-induced Ca^{2+} release and channel sensitivity to luminal Ca^{2+} activation are common defects of RyR2 mutations linked to ventricular tachycardia and sudden death. *Circ. Res.* **2005**, *97*, 1173–1181. [[CrossRef](#)] [[PubMed](#)]
24. Priori, S.G.; Chen, S.R.W. Inherited Dysfunction of Sarcoplasmic Reticulum Ca^{2+} Handling and Arrhythmogenesis. *Circ. Res.* **2011**, *108*, 871–883. [[CrossRef](#)]
25. Laver, D.R. Regulation of the RyR channel gating by Ca^{2+} and Mg^{2+} . *Biophys. Rev.* **2018**, *10*, 1087–1095. [[CrossRef](#)] [[PubMed](#)]
26. Sobie, E.A.; Dilly, K.W.; dos Santos Cruz, J.; Lederer, W.J.; Jafri, M.S. Termination of cardiac Ca^{2+} sparks: An investigative mathematical model of calcium-induced calcium release. *Biophys. J.* **2002**, *83*, 59–78. [[CrossRef](#)]
27. Cannell, M.B.; Kong, C.H.; Imtiaz, M.S.; Laver, D.R. Control of sarcoplasmic reticulum Ca^{2+} release by stochastic RyR gating within a 3D model of the cardiac dyad and importance of induction decay for CICR termination. *Biophys. J.* **2013**, *104*, 2149–2159. [[CrossRef](#)]
28. Walker, M.A.; Williams, G.S.B.; Kohl, T.; Lehnart, S.E.; Jafri, M.S.; Greenstein, J.L.; Lederer, W.J.; Winslow, R.L. Superresolution Modeling of Calcium Release in the Heart. *Biophys. J.* **2014**, *107*, 3018–3029. [[CrossRef](#)]
29. Stern, M.D.; Song, L.S.; Cheng, H.; Sham, J.S.; Yang, H.T.; Boheler, K.R.; Rios, E. Local control models of cardiac excitation-contraction coupling. A possible role for allosteric interactions between ryanodine receptors. *J. Gen. Physiol.* **1999**, *113*, 469–489. [[CrossRef](#)]
30. Stern, M.D.; Cheng, H. Putting out the fire: What terminates calcium-induced calcium release in cardiac muscle? *Cell Calcium* **2004**, *35*, 591–601. [[CrossRef](#)]
31. Stern, M.D.; Rios, E.; Maltsev, V.A. Life and death of a cardiac calcium spark. *J. Gen. Physiol.* **2013**, *142*, 257–274. [[CrossRef](#)]
32. Laver, D.R.; Kong, C.H.T.; Imtiaz, M.S.; Cannell, M.B. Termination of calcium-induced calcium release by induction decay: An emergent property of stochastic channel gating and molecular scale architecture. *J. Mol. Cell. Cardiol.* **2013**, *54*, 98–100. [[CrossRef](#)] [[PubMed](#)]
33. Winslow, R.L.; Greenstein, J.L. Extinguishing the sparks. *Biophys. J.* **2013**, *104*, 2115–2117. [[CrossRef](#)] [[PubMed](#)]

34. Song, Z.; Karma, A.; Weiss, J.N.; Qu, Z. Long-Lasting Sparks: Multi-Metastability and Release Competition in the Calcium Release Unit Network. *PLoS Comput. Biol.* **2016**, *12*, e1004671. [[CrossRef](#)] [[PubMed](#)]
35. Shannon, T.R.; Guo, T.; Bers, D.M. Ca²⁺ Scraps: Local Depletions of Free [Ca²⁺] in Cardiac Sarcoplasmic Reticulum During Contractions Leave Substantial Ca²⁺ Reserve. *Circ. Res.* **2003**, *93*, 40–45. [[CrossRef](#)]
36. Zima, A.V.; Picht, E.; Bers, D.M.; Blatter, L.A. Termination of cardiac Ca²⁺ sparks: Role of intra-SR [Ca²⁺], release flux, and intra-SR Ca²⁺ diffusion. *Circ. Res.* **2008**, *103*, e105–e115. [[CrossRef](#)]
37. Picht, E.; Zima, A.V.; Shannon, T.R.; Duncan, A.M.; Blatter, L.A.; Bers, D.M. Dynamic calcium movement inside cardiac sarcoplasmic reticulum during release. *Circ. Res.* **2011**, *108*, 847–856. [[CrossRef](#)]
38. Stern, M.D.; Pizarro, G.; Rios, E. Local control model of excitation-contraction coupling in skeletal muscle. *J. Gen. Physiol.* **1997**, *110*, 415–440. [[CrossRef](#)]
39. Shannon, T.R.; Wang, F.; Puglisi, J.; Weber, C.; Bers, D.M. A mathematical treatment of integrated Ca dynamics within the ventricular myocyte. *Biophys. J.* **2004**, *87*, 3351–3371. [[CrossRef](#)]
40. Restrepo, J.G.; Weiss, J.N.; Karma, A. Calsequestrin-mediated mechanism for cellular calcium transient alternans. *Biophys. J.* **2008**, *95*, 3767–3789. [[CrossRef](#)]
41. Keizer, J.; Levine, L. Ryanodine receptor adaptation and Ca²⁺-induced Ca²⁺ release-dependent Ca²⁺ oscillations. *Biophys. J.* **1996**, *71*, 3477–3487. [[CrossRef](#)]
42. Greenstein, J.L.; Winslow, R.L. An integrative model of the cardiac ventricular myocyte incorporating local control of Ca(2+) release. *Biophys. J.* **2002**, *83*, 2918–2945. [[CrossRef](#)]
43. Greene, D.A.; Shiferaw, Y. Mechanistic link between CaM-RyR2 interactions and the genesis of cardiac arrhythmia. *Biophys. J.* **2021**, *120*, 1469–1482. [[CrossRef](#)]
44. Wang, K.; Tu, Y.; Rappel, W.J.; Levine, H. Excitation-contraction coupling gain and cooperativity of the cardiac ryanodine receptor: A modeling approach. *Biophys. J.* **2005**, *89*, 3017–3025. [[CrossRef](#)] [[PubMed](#)]
45. Groff, J.R.; Smith, G.D. Ryanodine Receptor Allosteric Coupling and the Dynamics of Calcium Sparks. *Biophys. J.* **2008**, *95*, 135–154. [[CrossRef](#)] [[PubMed](#)]
46. Chen, W.; Wasserstrom, J.A.; Shiferaw, Y. Role of coupled gating between cardiac ryanodine receptors in the genesis of triggered arrhythmias. *Am. J. Physiol. Heart Circ. Physiol.* **2009**, *297*, H171–H180. [[CrossRef](#)]
47. Dixon, R.E.; Navedo, M.F.; Binder, M.D.; Santana, L.F. Mechanisms and physiological implications of cooperative gating of clustered ion channels. *Physiol. Rev.* **2022**, *102*, 1159–1210. [[CrossRef](#)]
48. Xiao, R.P.; Valdivia, H.H.; Bogdanov, K.; Valdivia, C.; Lakatta, E.G.; Cheng, H. The immunophilin FK506-binding protein modulates Ca²⁺ release channel closure in rat heart. *J. Physiol.* **1997**, *500*, 343–354. [[CrossRef](#)]
49. Zima, A.V.; Picht, E.; Bers, D.M.; Blatter, L.A. Partial inhibition of sarcoplasmic reticulum ca release evokes long-lasting ca release events in ventricular myocytes: Role of luminal ca in termination of ca release. *Biophys. J.* **2008**, *94*, 1867–1879. [[CrossRef](#)]
50. Picht, E.; DeSantiago, J.; Blatter, L.A.; Bers, D.M. Cardiac alternans do not rely on diastolic sarcoplasmic reticulum calcium content fluctuations. *Circ. Res.* **2006**, *99*, 740–748. [[CrossRef](#)]
51. Shkryl, V.M.; Maxwell, J.T.; Domeier, T.L.; Blatter, L.A. Refractoriness of sarcoplasmic reticulum Ca release determines Ca alternans in atrial myocytes. *Am. J. Physiol. Heart Circ. Physiol.* **2012**, *302*, H2310–H2320. [[CrossRef](#)]
52. Rovetti, R.; Cui, X.; Garfinkel, A.; Weiss, J.N.; Qu, Z. Spark-induced sparks as a mechanism of intracellular calcium alternans in cardiac myocytes. *Circ. Res.* **2010**, *106*, 1582–1591. [[CrossRef](#)] [[PubMed](#)]
53. Qu, Z.; Liu, M.B.; Nivala, M. A unified theory of calcium alternans in ventricular myocytes. *Sci. Rep.* **2016**, *6*, 35625. [[CrossRef](#)] [[PubMed](#)]
54. Zhong, X.; Sun, B.; Vallmitjana, A.; Mi, T.; Guo, W.; Ni, M.; Wang, R.; Guo, A.; Duff, H.J.; Gillis, A.M.; et al. Suppression of ryanodine receptor function prolongs Ca²⁺ release refractoriness and promotes cardiac alternans in intact hearts. *Biochem. J.* **2016**, *473*, 3951–3964. [[CrossRef](#)]
55. Sun, B.; Wei, J.; Zhong, X.; Guo, W.; Yao, J.; Wang, R.; Vallmitjana, A.; Benitez, R.; Hove-Madsen, L.; Chen, S.R.W. The cardiac ryanodine receptor, but not sarcoplasmic reticulum Ca²⁺-ATPase, is a major determinant of Ca²⁺ alternans in intact mouse hearts. *J. Biol. Chem.* **2018**, *293*, 13650–13661. [[CrossRef](#)]
56. Boyden, P.A.; Pu, J.; Pinto, J.; Keurs, H.E. Ca²⁺ transients and Ca²⁺ waves in purkinje cells: Role in action potential initiation. *Circ. Res.* **2000**, *86*, 448–455. [[CrossRef](#)] [[PubMed](#)]
57. Nivala, M.; Ko, C.Y.; Nivala, M.; Weiss, J.N.; Qu, Z. Criticality in intracellular calcium signaling in cardiac myocytes. *Biophys. J.* **2012**, *102*, 2433–2442. [[CrossRef](#)]
58. Nivala, M.; Ko, C.Y.; Nivala, M.; Weiss, J.N.; Qu, Z. The Emergence of Subcellular Pacemaker Sites for Calcium Waves and Oscillations. *J. Physiol.* **2013**, *591*, 5305–5320. [[CrossRef](#)] [[PubMed](#)]
59. Song, Z.; Qu, Z.; Karma, A. Stochastic initiation and termination of calcium-mediated triggered activity in cardiac myocytes. *Proc. Natl. Acad. Sci. USA* **2017**, *114*, E270–E279. [[CrossRef](#)] [[PubMed](#)]
60. Liu, N.; Denegri, M.; Dun, W.; Boncompagni, S.; Lodola, F.; Protasi, F.; Napolitano, C.; Boyden, P.A.; Priori, S.G. Abnormal Propagation of Calcium Waves and Ultrastructural Remodeling in Recessive Catecholaminergic Polymorphic Ventricular Tachycardia. *Circ. Res.* **2013**, *113*, 142–152. [[CrossRef](#)]
61. Stern, M.D. Theory of excitation-contraction coupling in cardiac muscle. *Biophys. J.* **1992**, *63*, 497–517. [[CrossRef](#)]

62. Smith, G.D.; Keizer, J.E.; Stern, M.D.; Lederer, W.J.; Cheng, H. A simple numerical model of calcium spark formation and detection in cardiac myocytes. *Biophys. J.* **1998**, *75*, 15–32. [[CrossRef](#)]
63. Hake, J.; Edwards, A.G.; Yu, Z.; Kekenus-Huskey, P.M.; Michailova, A.P.; McCammon, J.A.; Holst, M.J.; Hoshijima, M.; McCulloch, A.D. Modeling cardiac calcium sparks in a three-dimensional reconstruction of a calcium release unit. *J. Physiol.* **2012**, *590*, 4403–4422. [[CrossRef](#)] [[PubMed](#)]
64. Maltsev, A.V.; Maltsev, V.A.; Stern, M.D. Clusters of calcium release channels harness the Ising phase transition to confine their elementary intracellular signals. *Proc. Natl. Acad. Sci. USA* **2017**, *114*, 7525–7530. [[CrossRef](#)] [[PubMed](#)]
65. Gaur, N.; Rudy, Y. Multiscale modeling of calcium cycling in cardiac ventricular myocyte: Macroscopic consequences of microscopic dyadic function. *Biophys. J.* **2011**, *100*, 2904–2912. [[CrossRef](#)]
66. Nivala, M.; de Lange, E.; Rovetti, R.; Qu, Z. Computational modeling and numerical methods for spatiotemporal calcium cycling in ventricular myocytes. *Front. Physiol.* **2012**, *3*, 114. [[CrossRef](#)]
67. Colman, M.A.; Pinali, C.; Trafford, A.W.; Zhang, H.; Kitmitto, A. A computational model of spatio-temporal cardiac intracellular calcium handling with realistic structure and spatial flux distribution from sarcoplasmic reticulum and t-tubule reconstructions. *PLoS Comput. Biol.* **2017**, *13*, e1005714. [[CrossRef](#)]
68. Song, Z.; Liu, M.B.; Qu, Z. Transverse tubular network structures in the genesis of intracellular calcium alternans and triggered activity in cardiac cells. *J. Mol. Cell. Cardiol.* **2018**, *114*, 288–299. [[CrossRef](#)]
69. Hoang-Trong, T.M.; Ullah, A.; Lederer, W.J.; Jafri, M.S. A Stochastic Spatiotemporal Model of Rat Ventricular Myocyte Calcium Dynamics Demonstrated Necessary Features for Calcium Wave Propagation. *Membranes* **2021**, *11*, 989. [[CrossRef](#)]
70. Stanley, H.E. *Introduction to Phase Transitions and Critical Phenomena*; Oxford University Press: London, UK, 1971.
71. Stanley, H.E. Scaling, universality, and renormalization: Three pillars of modern critical phenomena. *Rev. Mod. Phys.* **1999**, *71*, S358–S366. [[CrossRef](#)]
72. Nivala, M.; Song, Z.; Weiss, J.N.; Qu, Z. T-tubule disruption promotes calcium alternans in failing ventricular myocytes: Mechanistic insights from computational modeling. *J. Mol. Cell. Cardiol.* **2015**, *79*, 32–41. [[CrossRef](#)]
73. Noble, D. A modification of the Hodgkin-Huxley equations applicable to Purkinje fibre action and pace-maker potentials. *J. Physiol.* **1962**, *160*, 317–352. [[CrossRef](#)] [[PubMed](#)]
74. Beeler, G.W.; Reuter, H. Reconstruction of the action potential of ventricular myocardial fibres. *J. Physiol.* **1977**, *268*, 177–210. [[CrossRef](#)] [[PubMed](#)]
75. Luo, C.H.; Rudy, Y. A model of the ventricular cardiac action potential: Depolarization, repolarization, and their interaction. *Circ. Res.* **1991**, *68*, 1501–1526. [[CrossRef](#)] [[PubMed](#)]
76. DiFrancesco, D.; Noble, D. A model of cardiac electrical activity incorporating ionic pumps and concentration changes. *Philos. Trans. R. Soc. Lond. (Biol.)* **1985**, *307*, 779–790.
77. Fabiato, A. Calcium-induced release of calcium from the cardiac sarcoplasmic reticulum. *Am. J. Physiol.* **1983**, *245*, C1–C14. [[CrossRef](#)]
78. Hilgemann, D.W.; Noble, D. Excitation-contraction coupling and extracellular calcium transients in rabbit atrium: Reconstruction of basic cellular mechanisms. *Proc. R. Soc. Lond. B Biol. Sci.* **1987**, *230*, 163–205.
79. Jafri, M.S.; Rice, J.J.; Winslow, R.L. Cardiac Ca²⁺ dynamics: The roles of ryanodine receptor adaptation and sarcoplasmic reticulum load. *Biophys. J.* **1998**, *74*, 1149–1168. [[CrossRef](#)]
80. Maltsev, V.A.; Lakatta, E.G. Synergism of coupled subsarcolemmal Ca²⁺ clocks and sarcolemmal voltage clocks confers robust and flexible pacemaker function in a novel pacemaker cell model. *Am. J. Physiol. Heart Circ. Physiol.* **2009**, *296*, H594–H615. [[CrossRef](#)]
81. Shannon, T.R.; Wang, F.; Bers, D.M. Regulation of Cardiac Sarcoplasmic Reticulum Ca Release by Luminal [Ca] and Altered Gating Assessed with a Mathematical Model. *Biophys. J.* **2005**, *89*, 4096–4110. [[CrossRef](#)]
82. Luo, C.H.; Rudy, Y. A dynamical model of the cardiac ventricular action potential: I. simulations of ionic currents and concentration changes. *Circ. Res.* **1994**, *74*, 1071–1096. [[CrossRef](#)]
83. Faber, G.M.; Rudy, Y. Action potential and contractility changes in [Na(+)](i) overloaded cardiac myocytes: A simulation study. *Biophys. J.* **2000**, *78*, 2392–2404. [[CrossRef](#)]
84. Chudin, E.; Goldhaber, J.; Garfinkel, A.; Weiss, J.; Kogan, B. Intracellular Ca²⁺ dynamics and the stability of ventricular tachycardia. *Biophys. J.* **1999**, *77*, 2930–2941. [[CrossRef](#)]
85. Fox, J.J.; McHarg, J.L.; Gilmour, R.F. Ionic mechanism of electrical alternans. *Am. J. Physiol. Heart Circ. Physiol.* **2002**, *282*, H516–H530. [[CrossRef](#)]
86. ten Tusscher, K.H.; Noble, D.; Noble, P.J.; Panfilov, A.V. A model for human ventricular tissue. *Am. J. Physiol. Heart Circ. Physiol.* **2004**, *286*, H1573–H1589. [[CrossRef](#)] [[PubMed](#)]
87. Hund, T.J.; Rudy, Y. Rate dependence and regulation of action potential and calcium transient in a canine cardiac ventricular cell model. *Circulation* **2004**, *110*, 3168–3174. [[CrossRef](#)]
88. Stewart, P.; Aslanidi, O.V.; Noble, D.; Noble, P.J.; Boyett, M.R.; Zhang, H. Mathematical models of the electrical action potential of Purkinje fibre cells. *Philos. Trans. A Math. Phys. Eng. Sci.* **2009**, *367*, 2225–2255. [[CrossRef](#)]
89. Livshitz, L.M.; Rudy, Y. Regulation of Ca²⁺ and electrical alternans in cardiac myocytes: Role of CAMKII and repolarizing currents. *Am. J. Physiol. Heart Circ. Physiol.* **2007**, *292*, H2854–H2866. [[CrossRef](#)] [[PubMed](#)]

90. O'Hara, T.; Virag, L.; Varro, A.; Rudy, Y. Simulation of the undiseased human cardiac ventricular action potential: Model formulation and experimental validation. *PLoS Comput. Biol.* **2011**, *7*, e1002061. [[CrossRef](#)] [[PubMed](#)]
91. Shiferaw, Y.; Watanabe, M.A.; Garfinkel, A.; Weiss, J.N.; Karma, A. Model of intracellular calcium cycling in ventricular myocytes. *Biophys. J.* **2003**, *85*, 3666–3686. [[CrossRef](#)]
92. Mahajan, A.; Shiferaw, Y.; Sato, D.; Baher, A.; Olcese, R.; Xie, L.-H.; Yang, M.-J.; Chen, P.-S.; Restrepo, J.G.; Karma, A.; et al. A rabbit ventricular action potential model replicating cardiac dynamics at rapid heart rates. *Biophys. J.* **2008**, *94*, 392–410. [[CrossRef](#)]
93. Bassani, J.W.; Yuan, W.; Bers, D.M. Fractional SR Ca release is regulated by trigger Ca and SR Ca content in cardiac myocytes. *Am. J. Physiol.* **1995**, *268*, C1313–C1319. [[CrossRef](#)] [[PubMed](#)]
94. Shannon, T.R.; Ginsburg, K.S.; Bers, D.M. Potentiation of fractional sarcoplasmic reticulum calcium release by total and free intra-sarcoplasmic reticulum calcium concentration. *Biophys. J.* **2000**, *78*, 334–343. [[CrossRef](#)]
95. Hinch, R.; Greenstein, J.L.; Tanskanen, A.J.; Xu, L.; Winslow, R.L. A simplified local control model of calcium-induced calcium release in cardiac ventricular myocytes. *Biophys. J.* **2004**, *87*, 3723–3736. [[CrossRef](#)] [[PubMed](#)]
96. Williams, G.S.; Huertas, M.A.; Sobie, E.A.; Jafri, M.S.; Smith, G.D. Moment closure for local control models of calcium-induced calcium release in cardiac myocytes. *Biophys. J.* **2008**, *95*, 1689–1703. [[CrossRef](#)]
97. Williams, G.S.B.; Huertas, M.A.; Sobie, E.A.; Jafri, M.S.; Smith, G.D. A Probability Density Approach to Modeling Local Control of Calcium-Induced Calcium Release in Cardiac Myocytes. *Biophys. J.* **2007**, *92*, 2311–2328. [[CrossRef](#)]
98. Huertas, M.A.; Smith, G.D.; Gyorke, S. Ca²⁺ alternans in a cardiac myocyte model that uses moment equations to represent heterogeneous junctional SR Ca²⁺. *Biophys. J.* **2010**, *99*, 377–387. [[CrossRef](#)]
99. Shiferaw, Y.; Aistrup, G.L.; Wasserstrom, J.A. Synchronization of triggered waves in atrial tissue. *Biophys. J.* **2018**, *115*, 1130–1141. [[CrossRef](#)]
100. Marchena, M.; Echebarria, B. Computational Model of Calcium Signaling in Cardiac Atrial Cells at the Submicron Scale. *Front. Physiol.* **2018**, *9*, 1760. [[CrossRef](#)]
101. Marchena, M.; Echebarria, B. Influence of the tubular network on the characteristics of calcium transients in cardiac myocytes. *PLoS ONE* **2020**, *15*, e0231056. [[CrossRef](#)]
102. Sutanto, H.; van Sloun, B.; Schönleitner, P.; van Zandvoort, M.A.M.J.; Antoons, G.; Heijman, J. The Subcellular Distribution of Ryanodine Receptors and L-Type Ca²⁺ Channels Modulates Ca²⁺-Transient Properties and Spontaneous Ca²⁺-Release Events in Atrial Cardiomyocytes. *Front. Physiol.* **2018**, *9*, 1108. [[CrossRef](#)]
103. Vagos, M.R.; Arevalo, H.; Heijman, J.; Schotten, U.; Sundnes, J. A Novel Computational Model of the Rabbit Atrial Cardiomyocyte with Spatial Calcium Dynamics. *Front. Physiol.* **2020**, *11*, 556156. [[CrossRef](#)] [[PubMed](#)]
104. Maltsev, A.V.; Yaniv, Y.; Stern, M.D.; Lakatta, E.G.; Maltsev, V.A. RyR-NCX-SERCA Local Cross-Talk Ensures Pacemaker Cell Function at Rest and During the Fight-or-Flight Reflex. *Circ. Res.* **2013**, *113*, e94–e100. [[CrossRef](#)] [[PubMed](#)]
105. Maltsev, A.V.; Maltsev, V.A.; Stern, M.D. Stabilization of diastolic calcium signal via calcium pump regulation of complex local calcium releases and transient decay in a computational model of cardiac pacemaker cell with individual release channels. *PLoS Comput. Biol.* **2017**, *13*, e1005675. [[CrossRef](#)]
106. Dibb, K.M.; Clarke, J.D.; Horn, M.A.; Richards, M.A.; Graham, H.K.; Eisner, D.A.; Trafford, A.W. Characterization of an Extensive Transverse Tubular Network in Sheep Atrial Myocytes and its Depletion in Heart Failure. *Circ. Heart Fail.* **2009**, *2*, 482–489. [[CrossRef](#)] [[PubMed](#)]
107. Brandenburg, S.; Kohl, T.; Williams, G.S.B.; Gusev, K.; Wagner, E.; Rog-Zielinska, E.A.; Heibisch, E.; Dura, M.; Didié, M.; Gotthardt, M.; et al. Axial tubule junctions control rapid calcium signaling in atria. *J. Clin. Investig.* **2016**, *126*, 3999–4015. [[CrossRef](#)] [[PubMed](#)]
108. Lyon, A.R.; MacLeod, K.T.; Zhang, Y.; Garcia, E.; Kanda, G.K.; Lab, M.J.; Korchev, Y.E.; Harding, S.E.; Gorelik, J. Loss of T-tubules and other changes to surface topography in ventricular myocytes from failing human and rat heart. *Proc. Natl. Acad. Sci. USA* **2009**, *106*, 6854–6859. [[CrossRef](#)]
109. Song, L.S.; Sobie, E.A.; McCulle, S.; Lederer, W.J.; Balke, C.W.; Cheng, H. Orphaned ryanodine receptors in the failing heart. *Proc. Natl. Acad. Sci. USA* **2006**, *103*, 4305–4310. [[CrossRef](#)]
110. Seidel, T.; Navankasattusas, S.; Ahmad, A.A.; Diakos, N.A.; Xu, W.D.; Tristani-Firouzi, M.; Bonios, M.; Taleb, I.; Li, D.Y.; Selzman, C.H.; et al. Sheet-Like Remodeling of the Transverse Tubular System in Human Heart Failure Impairs Excitation-Contraction Coupling and Functional Recovery by Mechanical Unloading. *Circulation* **2017**, *135*, 1632–1645. [[CrossRef](#)]
111. Chen, W.; Aistrup, G.; Wasserstrom, J.A.; Shiferaw, Y. A mathematical model of spontaneous calcium release in cardiac myocytes. *Am. J. Physiol. Heart Circ. Physiol.* **2011**, *300*, H1794–H1805. [[CrossRef](#)]
112. Gaeta, S.A.; Bub, G.; Abbott, G.W.; Christini, D.J. Dynamical mechanism for subcellular alternans in cardiac myocytes. *Circ. Res.* **2009**, *105*, 335–342. [[CrossRef](#)]
113. Sato, D.; Bers, D.M.; Shiferaw, Y. Formation of spatially discordant alternans due to fluctuations and diffusion of calcium. *PLoS ONE* **2014**, *8*, e85365. [[CrossRef](#)]
114. Li, Q.; O'Neill, S.C.; Tao, T.; Li, Y.; Eisner, D.; Zhang, H. Mechanisms by which cytoplasmic calcium wave propagation and alternans are generated in cardiac atrial myocytes lacking T-tubules—insights from a simulation study. *Biophys. J.* **2012**, *102*, 1471–1482. [[CrossRef](#)] [[PubMed](#)]
115. Tao, T.; O'Neill, S.C.; Diaz, M.E.; Li, Y.T.; Eisner, D.A.; Zhang, H. Alternans of cardiac calcium cycling in a cluster of ryanodine receptors: A simulation study. *Am. J. Physiol. Heart Circ. Physiol.* **2008**, *295*, H598–H609. [[CrossRef](#)] [[PubMed](#)]

116. Lou, Q.; Belevych, A.E.; Radwanski, P.B.; Liu, B.; Kalyanasundaram, A.; Knollmann, B.C.; Fedorov, V.V.; Gyorke, S. Alternating membrane potential/calcium interplay underlies repetitive focal activity in a genetic model of calcium-dependent atrial arrhythmias. *J. Physiol.* **2015**, *593*, 1443–1458. [[CrossRef](#)]
117. Belevych, A.E.; Terentyev, D.; Terentyeva, R.; Ho, H.T.; Gyorke, I.; Bonilla, I.M.; Carnes, C.A.; Billman, G.E.; Gyorke, S. Shortened Ca²⁺ signaling refractoriness underlies cellular arrhythmogenesis in a postinfarction model of sudden cardiac death. *Circ. Res.* **2012**, *110*, 569–577. [[CrossRef](#)] [[PubMed](#)]
118. Ko, C.Y.; Liu, M.B.; Song, Z.; Qu, Z.; Weiss, J.N. Multiscale Determinants of Delayed Afterdepolarization Amplitude in Cardiac Tissue. *Biophys. J.* **2017**, *112*, 1949–1961. [[CrossRef](#)]
119. Qu, Z.; Xie, L.-H.; Olcese, R.; Karagueuzian, H.S.; Chen, P.-S.; Garfinkel, A.; Weiss, J.N. Early afterdepolarizations in cardiac myocytes: Beyond reduced repolarization reserve. *Cardiovasc. Res.* **2013**, *99*, 6–15. [[CrossRef](#)]
120. Priori, S.G.; Corr, P.B. Mechanisms underlying early and delayed afterdepolarizations induced by catecholamines. *Am. J. Physiol.* **1990**, *258*, H1796–H1805. [[CrossRef](#)]
121. Volders, P.G.; Vos, M.A.; Szabo, B.; Sipido, K.R.; de Groot, S.H.; Gorgels, A.P.; Wellens, H.J.; Lazzara, R. Progress in the understanding of cardiac early afterdepolarizations and torsades de pointes: Time to revise current concepts. *Cardiovasc. Res.* **2000**, *46*, 376–392. [[CrossRef](#)]
122. Choi, B.R.; Burton, F.; Salama, G. Cytosolic Ca²⁺ triggers early afterdepolarizations and Torsade de Pointes in rabbit hearts with type 2 long QT syndrome. *J. Physiol.* **2002**, *543*, 615–631. [[CrossRef](#)]
123. Zhao, Z.; Wen, H.; Fefelova, N.; Allen, C.; Baba, A.; Matsuda, T.; Xie, L.H. Revisiting the ionic mechanisms of early afterdepolarizations in cardiomyocytes: Predominant by Ca waves or Ca currents? *Am. J. Physiol. Heart Circ. Physiol.* **2012**, *302*, H1636–H1644. [[CrossRef](#)] [[PubMed](#)]
124. Song, Z.; Ko, C.Y.; Nivala, M.; Weiss, J.N.; Qu, Z. Calcium-Voltage Coupling in the Genesis of Early and Delayed Afterdepolarizations in Cardiac Myocytes. *Biophys. J.* **2015**, *108*, 1908–1921. [[CrossRef](#)]
125. Zhong, M.; Rees, C.M.; Terentyev, D.; Choi, B.-R.; Koren, G.; Karma, A. NCX-Mediated Subcellular Ca²⁺ Dynamics Underlying Early Afterdepolarizations in LQT2 Cardiomyocytes. *Biophys. J.* **2018**, *115*, 1019–1032. [[CrossRef](#)] [[PubMed](#)]
126. Wilson, D.; Ermentrout, B.; Nemeč, J.; Salama, G. A model of cardiac ryanodine receptor gating predicts experimental Ca²⁺-dynamics and Ca²⁺-triggered arrhythmia in the long QT syndrome. *Chaos Interdiscip. J. Nonlinear Sci.* **2017**, *27*, 093940. [[CrossRef](#)] [[PubMed](#)]
127. Huang, X.; Song, Z.; Qu, Z. Determinants of early afterdepolarization properties in ventricular myocyte models. *PLoS Comput. Biol.* **2018**, *14*, e1006382. [[CrossRef](#)]
128. Brown, D.A.; O'Rourke, B. Cardiac mitochondria and arrhythmias. *Cardiovasc. Res.* **2010**, *88*, 241–249. [[CrossRef](#)]
129. Ruiz-Meana, M.; Fernandez-Sanz, C.; Garcia-Dorado, D. The SR-mitochondria interaction: A new player in cardiac pathophysiology. *Cardiovasc. Res.* **2010**, *88*, 30–39. [[CrossRef](#)]
130. Cortassa, S.; Aon, M.A.; Marban, E.; Winslow, R.L.; O'Rourke, B. An integrated model of cardiac mitochondrial energy metabolism and calcium dynamics. *Biophys. J.* **2003**, *84*, 2734–2755. [[CrossRef](#)]
131. Cortassa, S.; Aon, M.A.; O'Rourke, B.; Jacques, R.; Tseng, H.J.; Marban, E.; Winslow, R.L. A computational model integrating electrophysiology, contraction, and mitochondrial bioenergetics in the ventricular myocyte. *Biophys. J.* **2006**, *91*, 1564–1589. [[CrossRef](#)]
132. Zhou, L.; Cortassa, S.; Wei, A.-C.; Aon, M.A.; Winslow, R.L.; O'Rourke, B. Modeling Cardiac Action Potential Shortening Driven by Oxidative Stress-Induced Mitochondrial Oscillations in Guinea Pig Cardiomyocytes. *Biophys. J.* **2009**, *97*, 1843–1852. [[CrossRef](#)]
133. Matsuoka, S.; Sarai, N.; Jo, H.; Noma, A. Simulation of ATP metabolism in cardiac excitation-contraction coupling. *Prog. Biophys. Mol. Biol.* **2004**, *85*, 279–299. [[CrossRef](#)] [[PubMed](#)]
134. Takeuchi, A.; Kim, B.; Matsuoka, S. The mitochondrial Na⁺-Ca²⁺ exchanger, NCLX, regulates automaticity of HL-1 cardiomyocytes. *Sci. Rep.* **2013**, *3*, 2766. [[CrossRef](#)]
135. Aon, M.A.; Cortassa, S.; O'Rourke, B. Percolation and criticality in a mitochondrial network. *Proc. Natl. Acad. Sci. USA* **2004**, *101*, 4447–4452. [[CrossRef](#)] [[PubMed](#)]
136. Nivala, M.; Korge, P.; Nivala, M.; Weiss, J.N.; Qu, Z. Linking flickering to waves and whole-cell oscillations in a mitochondrial network model. *Biophys. J.* **2011**, *101*, 2102–2111. [[CrossRef](#)] [[PubMed](#)]
137. Pandey, V.; Xie, L.H.; Qu, Z.; Song, Z. Mitochondrial depolarization promotes calcium alternans: Mechanistic insights from a ventricular myocyte model. *PLoS Comput. Biol.* **2021**, *17*, e1008624. [[CrossRef](#)] [[PubMed](#)]
138. Song, Z.; Xie, L.-H.; Weiss, J.N.; Qu, Z. A spatiotemporal ventricular myocyte model incorporating mitochondrial calcium cycling. *Biophys. J.* **2019**, *117*, 2349–2360. [[CrossRef](#)]
139. Xie, A.; Song, Z.; Liu, H.; Zhou, A.; Shi, G.; Wang, Q.; Gu, L.; Liu, M.; Xie, L.H.; Qu, Z.; et al. Mitochondrial Ca²⁺ Influx Contributes to Arrhythmic Risk in Nonischemic Cardiomyopathy. *J. Am. Heart Assoc.* **2018**, *7*, e007805. [[CrossRef](#)]
140. Pandey, V.; Xie, L.-H.; Qu, Z.; Song, Z. Mitochondrial Contributions in the Genesis of Delayed Afterdepolarizations in Ventricular Myocytes. *Front. Physiol.* **2021**, *12*, 1631. [[CrossRef](#)]
141. Bers, D.M. Calcium cycling and signaling in cardiac myocytes. *Annu. Rev. Physiol.* **2008**, *70*, 23–49. [[CrossRef](#)]
142. Saucerman, J.J.; Brunton, L.L.; Michailova, A.P.; McCulloch, A.D. Modeling beta-adrenergic control of cardiac myocyte contractility in silico. *J. Biol. Chem.* **2003**, *278*, 47997–48003. [[CrossRef](#)]

143. Xie, Y.; Grandi, E.; Puglisi, J.L.; Sato, D.; Bers, D.M. beta-adrenergic stimulation activates early afterdepolarizations transiently via kinetic mismatch of PKA targets. *J. Mol. Cell. Cardiol.* **2013**, *58*, 153–161. [[CrossRef](#)]
144. Hashambhoy, Y.L.; Greenstein, J.L.; Winslow, R.L. Role of CaMKII in RyR leak, EC coupling and action potential duration: A computational model. *J. Mol. Cell. Cardiol.* **2010**, *49*, 617–624. [[CrossRef](#)] [[PubMed](#)]
145. Hashambhoy, Y.L.; Winslow, R.L.; Greenstein, J.L. CaMKII-induced shift in modal gating explains L-type Ca(2+) current facilitation: A modeling study. *Biophys. J.* **2009**, *96*, 1770–1785. [[CrossRef](#)] [[PubMed](#)]
146. Foteinou, P.T.; Greenstein, J.L.; Winslow, R.L. Mechanistic Investigation of the Arrhythmogenic Role of Oxidized CaMKII in the Heart. *Biophys. J.* **2015**, *109*, 838–849. [[CrossRef](#)] [[PubMed](#)]
147. Liu, M.B.; de Lange, E.; Garfinkel, A.; Weiss, J.N.; Qu, Z. Delayed afterdepolarizations generate both triggers and a vulnerable substrate promoting reentry in cardiac tissue. *Heart Rhythm* **2015**, *12*, 2115–2124. [[CrossRef](#)] [[PubMed](#)]
148. Campos, F.O.; Shiferaw, Y.; Prassl, A.J.; Boyle, P.M.; Vigmond, E.J.; Plank, G. Stochastic spontaneous calcium release events trigger premature ventricular complexes by overcoming electrotonic load. *Cardiovasc. Res.* **2015**, *107*, 175–183. [[CrossRef](#)]
149. Colman, M.A. Arrhythmia mechanisms and spontaneous calcium release: Bi-directional coupling between re-entrant and focal excitation. *PLoS Comput. Biol.* **2019**, *15*, e1007260. [[CrossRef](#)]
150. Colman, M.A.; Holmes, M.; Whittaker, D.G.; Jayasinghe, I.; Benson, A.P. Multi-scale approaches for the simulation of cardiac electrophysiology: I—Sub-cellular and stochastic calcium dynamics from cell to organ. *Methods* **2020**, *185*, 49–59. [[CrossRef](#)] [[PubMed](#)]
151. Greene, D.A.; Kaboudian, A.; Wasserstrom, J.A.; Fenton, F.H.; Shiferaw, Y. Voltage-mediated mechanism for calcium wave synchronization and arrhythmogenesis in atrial tissue. *Biophys. J.* **2022**, *121*, 383–395. [[CrossRef](#)] [[PubMed](#)]
152. Walker, M.A.; Gurev, V.; Rice, J.J.; Greenstein, J.L.; Winslow, R.L. Estimating the probabilities of rare arrhythmic events in multiscale computational models of cardiac cells and tissue. *PLoS Comput. Biol.* **2017**, *13*, e1005783. [[CrossRef](#)]
153. Xie, F.; Qu, Z.; Yang, J.; Baher, A.; Weiss, J.N.; Garfinkel, A. A simulation study of the effects of cardiac anatomy in ventricular fibrillation. *J. Clin. Investig.* **2004**, *113*, 686–693. [[PubMed](#)]
154. Ten Tusscher, K.H.; Hren, R.; Panfilov, A.V. Organization of ventricular fibrillation in the human heart. *Circ. Res.* **2007**, *100*, e87–e101. [[CrossRef](#)] [[PubMed](#)]
155. Liu, M.B.; Vandersickel, N.; Panfilov, A.V.; Qu, Z. R-from-T as a common mechanism of arrhythmia initiation in long QT syndromes. *Circ. Arrhythm. Electrophysiol.* **2019**, *12*, e007571. [[CrossRef](#)] [[PubMed](#)]
156. Keener, J.P. The effects of discrete gap junction coupling on propagation in myocardium. *J. Theor. Biol.* **1991**, *148*, 49–82. [[CrossRef](#)]
157. Qu, Z.; Karagueuzian, H.S.; Garfinkel, A.; Weiss, J.N. Effects of Na⁺ channel and cell coupling abnormalities on vulnerability to reentry: A simulation study. *Am. J. Physiol. Heart Circ. Physiol.* **2004**, *286*, H1310–H1321. [[CrossRef](#)]
158. Huang, C.; Song, Z.; Qu, Z. Synchronization of spatially discordant voltage and calcium alternans in cardiac tissue. *Phys. Rev. E* **2022**, *106*, 024406. [[CrossRef](#)]
159. Greenstein, J.L.; Winslow, R.L. Integrative systems models of cardiac excitation-contraction coupling. *Circ. Res.* **2011**, *108*, 70–84. [[CrossRef](#)]
160. Rice, J.J.; Jafri, M.S.; Winslow, R.L. Modeling short-term interval-force relations in cardiac muscle. *Am. J. Physiol. Heart Circ. Physiol.* **2000**, *278*, H913–H931. [[CrossRef](#)]
161. Rice, J.J.; Winslow, R.L.; Hunter, W.C. Comparison of putative cooperative mechanisms in cardiac muscle: Length dependence and dynamic responses. *Am. J. Physiol.* **1999**, *276*, H1734–H1754. [[CrossRef](#)]
162. Silva, J.R.; Pan, H.; Wu, D.; Nekouzadeh, A.; Decker, K.F.; Cui, J.; Baker, N.A.; Sept, D.; Rudy, Y. A multiscale model linking ion-channel molecular dynamics and electrostatics to the cardiac action potential. *Proc. Natl. Acad. Sci. USA* **2009**, *106*, 11102–11106. [[CrossRef](#)]
163. Yang, P.C.; DeMarco, K.R.; Aghasafari, P.; Jeng, M.T.; Dawson, J.R.D.; Bekker, S.; Noskov, S.Y.; Yarov-Yarovoy, V.; Vorobyov, I.; Clancy, C.E. A Computational Pipeline to Predict Cardiotoxicity: From the Atom to the Rhythm. *Circ. Res.* **2020**, *126*, 947–964. [[CrossRef](#)] [[PubMed](#)]
164. Jensen, M.Ø.; Borhani, D.W.; Lindorff-Larsen, K.; Maragakis, P.; Jogini, V.; Eastwood, M.P.; Dror, R.O.; Shaw, D.E. Principles of conduction and hydrophobic gating in K⁺ channels. *Proc. Natl. Acad. Sci. USA* **2010**, *107*, 5833–5838. [[CrossRef](#)] [[PubMed](#)]
165. Qu, Z.; Garfinkel, A.; Weiss, J.N.; Nivala, M. Multi-scale modeling in biology: How to bridge the gaps between scales? *Prog. Biophys. Mol. Biol.* **2011**, *107*, 21–31. [[CrossRef](#)] [[PubMed](#)]
166. Fox, R.F. Stochastic versions of the Hodgkin-Huxley equations. *Biophys. J.* **1997**, *72*, 2068–2074. [[CrossRef](#)]
167. Keener, J.P. Invariant manifold reductions for Markovian ion channel dynamics. *J. Math. Biol.* **2009**, *58*, 447–457. [[CrossRef](#)]
168. Landaw, J.; Qu, Z. Bifurcations Caused by Feedback between Voltage and Intracellular Ion Concentrations in Ventricular Myocytes. *Phys. Rev. Lett.* **2019**, *123*, 218101. [[CrossRef](#)]
169. Qu, Z.; Shiferaw, Y.; Weiss, J.N. Nonlinear dynamics of cardiac excitation-contraction coupling: An iterated map study. *Phys. Rev. E* **2007**, *75*, 011927. [[CrossRef](#)]